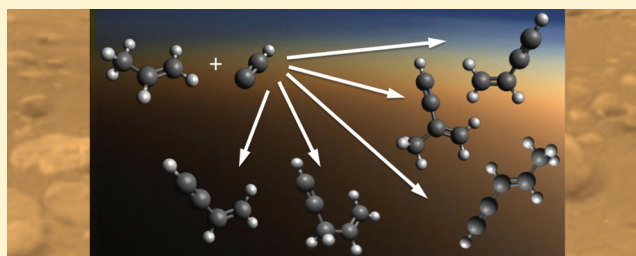


Bimolecular Rate Constant and Product Branching Ratio Measurements for the Reaction of C_2H with Ethene and Propene at 79 KJordy Bouwman,[†] Fabien Goulay,^{†,§} Stephen R. Leone,^{†,‡} and Kevin R. Wilson^{*,‡}[†]Departments of Chemistry and Physics, University of California Berkeley, Berkeley, California 94720, United States[‡]Chemical Sciences Division, Lawrence Berkeley National Laboratory, 1 Cyclotron Road, Berkeley, California 94720, United States

ABSTRACT: The reactions of the ethynyl radical (C_2H) with ethene (C_2H_4) and propene (C_3H_6) are studied under low temperature conditions (79 K) in a pulsed Laval nozzle apparatus. Ethynyl radicals are formed by 193 nm photolysis of acetylene (C_2H_2) and the reactions are studied in nitrogen as a carrier gas. Reaction products are sampled and subsequently photoionized by the tunable vacuum ultraviolet radiation of the Advanced Light Source (ALS) at Lawrence Berkeley National Laboratory. The product ions are detected mass selectively and time-resolved by a quadrupole mass spectrometer. Bimolecular rate coefficients are determined under pseudo-first-order conditions, yielding values in good agreement with previous measurements. Photoionization spectra are measured by scanning the ALS photon energy while detecting the ionized reaction products. Analysis of the photoionization spectra yields—for the first time—low temperature isomer resolved product branching ratios. The reaction between C_2H and ethene is found to proceed by H-loss and yields 100% vinylacetylene. The reaction between C_2H and propene results in $(85 \pm 10)\%$ C_4H_4 ($m/z = 52$) via CH_3 -loss and $(15 \pm 10)\%$ C_5H_6 ($m/z = 66$) by H-loss. The C_4H_4 channel is found to consist of 100% vinylacetylene. For the C_5H_6 channel, analysis of the photoionization spectrum reveals that $(62 \pm 16)\%$ is in the form of 4-penten-1-yne, $(27 \pm 8)\%$ is in the form of *cis*- and *trans*-3-penten-1-yne and $(11 \pm 10)\%$ is in the form of 2-methyl-1-buten-3-yne.



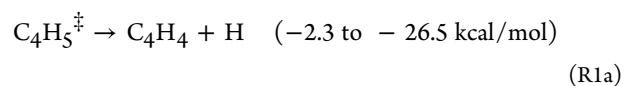
■ INTRODUCTION

The reactive ethynyl (C_2H) radical plays a crucial role in the complex chemistries of planetary atmospheres, such as that of Saturn's largest moon, Titan.^{1–4} Titan's atmosphere is cold ($T = 70$ – 180 K) and dense,⁵ and it consists of mostly nitrogen ($>98\%$) with trace amounts of hydrocarbons.⁶ C_2H radicals are formed through the UV photolysis of acetylene (C_2H_2) by solar radiation.^{7,8} Subsequent reactions of C_2H with small unsaturated hydrocarbon species result in molecular growth,^{9–11} leading to larger polyynes, aromatic molecules, and aerosols that are thought to make up the haze that shrouds the moon.^{12–14} The C_2H radical is also ubiquitous in the interstellar medium^{15,16} and is considered to be a central species in the formation of the polycyclic aromatic hydrocarbons (PAHs) in outflows of carbon rich stars.^{17,18}

Trace amounts of ethene (C_2H_4) have been detected in Titan's stratosphere through mid-IR observations by the Voyager I mission and later by the Infrared Space Observatory (ISO).^{19,20} Propene (C_3H_6) has been identified in Titan's ionosphere by Cassini's Ion Neutral Mass Spectrometer (INMS)²¹ and is also expected to be present in Titan's lower atmosphere, where photoinduced processes dominate the neutral chemistry.^{2–4} Both ethene and propene are predicted to play a key role in the evolution of the chemical constituents of Titan's atmosphere.^{3,4,22} Thus, accurate reaction rate constants and isomer-specific product distributions of ethene and propene reacting with C_2H under Titan-relevant conditions are needed for accurate modeling of Titan's atmospheric chemistry.

Over the past few decades, Laval nozzle expansions have been employed by a number of groups to measure low temperature bimolecular reaction rate constants of radical-neutral reactions.^{23–28} Typically, these systems employ laser induced fluorescence or chemiluminescence to measure the decay rate of a radical species as a function of reactant density. In this manner, the bimolecular reaction rate constants for ethene^{29–31} and propene^{30,31} reacting with C_2H have been measured experimentally at Titan-relevant temperatures and are found to be near the collision limit. Based on the lack of pressure dependence, the slightly negative temperature dependence, and thermodynamic considerations, it was argued that these reactions proceed via an addition–elimination mechanism.^{29–31} Currently, the distribution of products from these reactions under Titan-relevant conditions cannot be retrieved via the optically based methods used to quantify these low temperature rate coefficients.

Theory predicts that two exit channels are thermodynamically accessible for the reaction between ethene and ethynyl³²

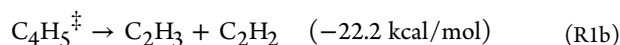


Received: January 31, 2012

Revised: March 18, 2012

Published: March 19, 2012

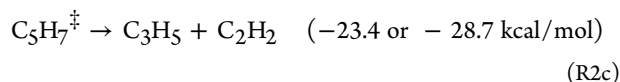
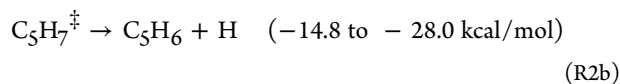
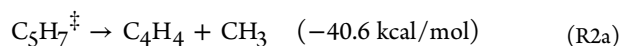




The range of exothermicities associated with the formation of C_4H_4 denotes the formation of the three C_4H_4 isomers vinylacetylene, butatriene and methylenecyclopropene. The $\text{C}_2\text{H}_3 + \text{C}_2\text{H}_2$ product channel R1b is accessible through an addition–elimination process on the C_4H_5 potential energy surface. This is found to be highly improbable, since multiple steps are required.³² Alternatively, this product channel can be reached directly by hydrogen abstraction. This pathway is also unlikely to contribute at Titan-relevant temperatures, since there is a barrier of 1.4 kcal/mol (~ 470 K) associated with it.³³ The most probable pathway is the formation of the C_4H_4 isomer vinylacetylene R1a, which is exothermic by 26.5 kcal/mol.^{32,34}

Zhang et al.³⁵ performed a crossed molecular beam study on the reaction between C_2H ($X^2\Sigma^+$) and C_2H_4 at high collision energy ($E = 4.92 \text{ kcal mol}^{-1}$). They found that vinylacetylene is the sole product formed from this reaction. Kovács et al.⁸ studied the reaction between C_2H and C_2H_4 in a slow flow excimer laser flash photolysis setup at room temperature and at pressures between 23 and 81 Torr. They quantified the H-atom yield by a Vacuum Ultraviolet (VUV) Ly- α laser induced fluorescence scheme and found that the yield of H-atoms from this reaction is close to unity, implying that the C_4H_4 isomer vinylacetylene is the sole reaction product. No low temperature product detection data are available for this reaction.

Theory predicts that from the reaction between C_2H and propene an energetic C_5H_7 adduct species is formed without a barrier. The adduct subsequently isomerizes by H-atom, methyl (CH_3) or C_3H_5 elimination to form stable reaction products:³⁴



The ranges of exothermicities for the formation of C_5H_6 depicts the formation of the isomers *trans*-penten-1-yne, *cis*-3-penten-1-yne, 2-methyl-1-buten-3-yne, 4-penten-1-yne, and cyclopropylacetylene. The two energies associated with R2c denote the formation of two isomers of the C_3H_5 radical. Direct hydrogen abstraction by C_2H from propene is expected to proceed via a barrier³³ and this reaction path is thus unlikely to contribute at low temperatures. The formation of $\text{C}_2\text{H}_2 + \text{C}_3\text{H}_5$ via an addition–elimination pathway R2c, however, is feasible.

The reaction between C_2H and propene has been studied experimentally by monitoring the H-atoms originating from the reaction at room temperature.⁸ From their experiments, Kovács et al.⁸ detected no H-atoms and derived an upper limit of 5% for the hydrogen loss channel R2a. They point out three possible explanations for the nondetection of hydrogen atoms: (i) Collisional stabilization of the adduct, (ii) 1,2-hydrogen migration within the adduct, thereby forming the $(\text{CH}_3)\text{CH}_2\text{C}\cdot\text{HCCH}$ species, is more rapid than H-elimination from the adduct. Subsequent methyl loss from the $(\text{CH}_3)\text{CH}_2\text{C}\cdot\text{H}-\text{CCH}$ radical produces C_4H_4 , and (iii) Direct H-abstraction to form the resonantly stabilized allyl radical. To date, no product detection or product branching measurements at any temperature are available to test their hypothesis.

Woon and Park³⁴ attempted to predict—under Titan-relevant conditions—the product branching ratios of species formed from reactions between C_2H and a set of alkenes, including ethene and propene. By means of large basis set DFT calculations in conjunction with a multiple-well treatment, they found that vinylacetylene is the dominant reaction product from C_2H reacting with both ethene and propene. Furthermore, they predict that the C_3H_6 species formed from the H-loss channel from C_2H reacting with propene can consist of a set of different isomers.³⁴

Here we present, for the first time, low-temperature isomer specific product branching ratios measured by mass spectrometry for the C_2H radical reacting with ethene and propene. Reaction products are identified and quantified by modeling the measured photoionization spectra using absolute photoionization spectra from the literature and DFT computed photoionization spectra of possible isomers. Additionally, bimolecular rate coefficients have been measured for both reactions by analyzing the time-resolved formation of the product species. The reaction rate coefficients are compared with previously measured values. The implications of the branching ratios for Titan's hydrocarbon chemistry are highlighted.

■ EXPERIMENTAL SECTION

Measurements are performed in a pulsed Laval nozzle apparatus coupled to tunable VUV synchrotron radiation from the Advanced Light Source (ALS) at Lawrence Berkeley National Laboratory. The experimental setup has been described in detail in a previous publication³⁶ and will be described only briefly here.

Laval expansion. A Laval nozzle, designed to yield a Mach 4 expansion, is mounted inside a vacuum chamber on a reservoir block that is filled with gas by two pulsed solenoid valves. The vacuum chamber is pumped down by a roots blower and the pressure in the vacuum chamber during Laval operation is maintained at 145 mTorr by a feedforward-loop controlled butterfly valve mounted on the intake of the roots blower. A flow of nitrogen slip gas is maintained to reduce pressure fluctuations during Laval operation. The system runs at a repetition rate of 10 Hz with a gas pulse duration of 5 ms.

Acetylene (C_2H_2 , Airgas, stabilized by acetone) is used as the C_2H precursor gas and is passed through a charcoal cartridge filter to remove the acetone. Nitrogen boil off from a liquid N_2 dewar is used as the carrier gas. The reactant gases ethene (C_2H_4 , Airgas, 99%) and propene (C_3H_6 , Sigma Aldrich, $\geq 99\%$) are used as commercially available. The acetylene, nitrogen, and reactant gas are supplied to the Laval nozzle through individual calibrated mass flow controllers. A cylinder is mounted between the mass flow controllers and the nozzle assembly to ensure good mixing of the radical precursor, reactant and bath gas.

A calibrated pressure transducer is mounted on the Laval nozzle reservoir block to monitor the stagnation pressure in the reservoir during the expansion. The Laval nozzle assembly is mounted on a stepper-motor-controlled movable linear translator and the position of the nozzle can be controlled by means of a LabView program. A second pressure transducer is mounted in the vacuum chamber and can be manually inserted into the flow perpendicular to the expanding gas. The resulting setup allows for accurate determination of both the uniformity of the expansion as well as the temperature of the expanding gas as described in detail by Sims et al.³⁷ The temperature is found to be 79 K with variations smaller than ± 2 K.

Ethynyl radicals (C_2H) are formed from the acetylene precursor by coaxially pulsing an unfocused ArF excimer laser

(193 nm) through the collimated expansion. This method is known to yield vibrationally and electronically excited C_2H radicals, but these are rapidly quenched in the expansion.³⁸ The absorption cross section³⁹ of C_2H_2 at 193 nm is $2 \times 10^{-19} \text{ cm}^2$ and the quantum yield of C_2H radicals is unity⁸ resulting in a number density of C_2H radicals of $\sim 8 \times 10^{10} \text{ cm}^{-3}$. Number densities of the reactant species, $[R]$, range from $1 \times 10^{13} \text{ cm}^{-3}$ to $25 \times 10^{13} \text{ cm}^{-3}$, so that the kinetic measurements are performed under pseudofirst-order conditions ($[C_2H] \ll [R]$).

Product Detection. Part of the collimated expansion is sampled through a $450 \mu\text{m}$ pinhole in a parabolically shaped airfoil mounted downward of the expansion. During an experiment, the region after the pinhole sampling is kept at high vacuum ($\sim 10^{-7}$ Torr) by two 2000 L/s turbomolecular pumps. The molecular beam formed after the pinhole is ionized with the quasi-continuous tunable radiation from the ALS. The resulting ions are extracted and mass selectively detected using a Quadrupole Mass Spectrometer (QMS). The ion counts measured by the QMS are recorded as a function of time using a multichannel scaler. For the kinetic measurements, ion counts vs time are recorded for 5,000 laser pulses to obtain a kinetic trace at a single reactant density setting. The time resolution of the kinetic measurements is determined by the QMS response function. The QMS response function is quantified by measuring the instantaneous formation of vinyl (C_2H_3) and methyl (CH_3) radicals upon 193 nm excimer laser photolysis of propene. The response of the QMS is found to be well represented by a Gaussian profile with a Full-Width-at-Half-Maximum (fwhm) of 15 μs .

The ionizing radiation from the ALS is dispersed in a 3 m monochromator and a portion of the dispersed light enters the ionization region through a $600 \mu\text{m}$ slit, resulting in an energy resolution of approximately 25 meV. For the measurements of photoionization spectra described here, the energy of the ionizing radiation is scanned from ~ 8 to 11.3 eV, while detecting the ion counts in a single mass channel. Ion counts are typically time binned for 600 laser pulses for each synchrotron photon energy. Subsequently, the ion counts are corrected for the photon energy dependent flux of the ALS, which is measured with a NIST calibrated VUV photodiode.

The mass dependent sensitivity of the quadrupole mass spectrometer detector is measured, which is essential for determining the absolute branching ratio for reactions with multiple product channels. This is done by measuring the response of the QMS detector to a calibration gas mixture containing accurate concentrations of species for which the ionization cross sections are well established (CH_4 , 1%, $\sigma_{15\text{eV}} = 25.4 \text{ MB}$,⁴⁰ with $1 \text{ MB} = 10^{-18} \text{ cm}^2$, Kr, 0.5%, $\sigma_{15\text{eV}} = 45.0 \text{ MB}$,⁴¹ and Xe, 1%, $\sigma_{15\text{eV}} = 61.1 \text{ MB}$ ⁴¹). The detected ion counts $S_i^{\text{det}}(E)$ for species i at photon energy E can be written as

$$S_i^{\text{det}}(E) = \Lambda \sigma_i(E) N_i \alpha_i \quad (1)$$

where Λ is a mass-independent instrument response function, which includes the geometry of the ionization region, photon flux and signal averaging. $\sigma_i(E)$ is the absolute ionization cross section of species i as a function of energy, and N_i is the concentration of the species in the gas expansion corrected for the fractional natural abundance of i . α_i is the mass discrimination factor of the QMS, which includes the

channeltron efficiency. Assuming that the mass discrimination can be described by the polynomial:⁴²

$$\alpha_i = A + Bm_i + Cm_i^2 \quad (2)$$

with m_i the mass of species i , eq 1 can be rewritten as

$$S_i^{\text{cor}}(E) = \frac{S_i^{\text{det}}(E)}{\sigma_i(E)N_i} = \Lambda(A + Bm_i + Cm_i^2) \quad (3)$$

where $S_i^{\text{cor}}(E)$ is the signal corrected for cross sections $\sigma_i(E)$ and isotopic fractions N_i .

In Figure 1, the values of $S_i^{\text{cor}}(E)$ measured at an ionization energy of 15 eV and normalized to the value at $m/z = 16$ are displayed against mass of methane, krypton and xenon. The figure shows that the sensitivity curve is fairly flat with slightly higher sensitivity toward the lower masses, which is common for quadrupole mass spectrometers.⁴² The polynomial fit to the corrected signal is also displayed in Figure 1. This curve is later

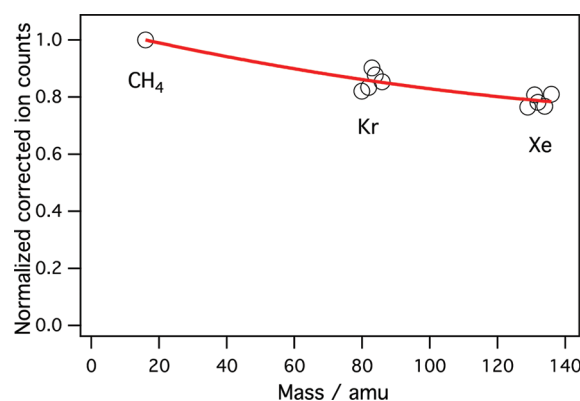


Figure 1. Ionization cross section and isotopic-fractions-corrected photoionization signal of methane, krypton and xenon at 15 eV photon energy, normalized to the signal at $m/z = 16$.

used to correct for the QMS sensitivity for determining absolute branching ratios between product channels.

Computational Method. Measured photoionization spectra are modeled with photoionization spectra from the literature to identify products and to obtain branching ratios. The overall shape and onset of a photoionization spectrum of likely reaction products, for which no photoionization data are available from the literature, are simulated by calculating oscillator strengths within the Franck–Condon approximation. To this end, electronic structures are calculated for the ground state and ionized species with the *Gaussian 03* package.⁴³ The CBS-QB3 method of Petersson and co-workers^{44,45} is used to obtain reliable energies, optimized bond distances, force constants and frequencies. Transition probabilities from the neutral ground state to the ionized ground state are computed, including full Duschinsky rotation for all symmetric modes, with the *PESCAL* package.^{46,47} The calculated spectra are convoluted with the ALS resolution of 25 meV and subsequently integrated, resulting in photoionization spectra. Absolute absorption cross sections are estimated using the method developed by Bobeldijk et al.⁴⁸

RESULTS AND DISCUSSION

Low Temperature Product Detection. Figure 2A shows an image of the ion counts detected by the QMS as a function of mass and time obtained for the reaction between C_2H and

propene. The image is composed of time traces that are recorded by stepping through the mass channels of the QMS with a resolution of 0.1 amu. The product species are ionized at a synchrotron photon energy of 11.25 eV prior to being detected. Each individual time trace is recorded by time binning the ion counts for 200 laser pulses. The horizontal line of high ion counts at $t \approx -40 \mu\text{s}$ is caused by the photolysis laser and shows when the reaction is initiated.

Figure 2B shows a vertical slice of the image integrated from $m/z = 51.5$ to 52.5 . The resulting trace depicts the formation of

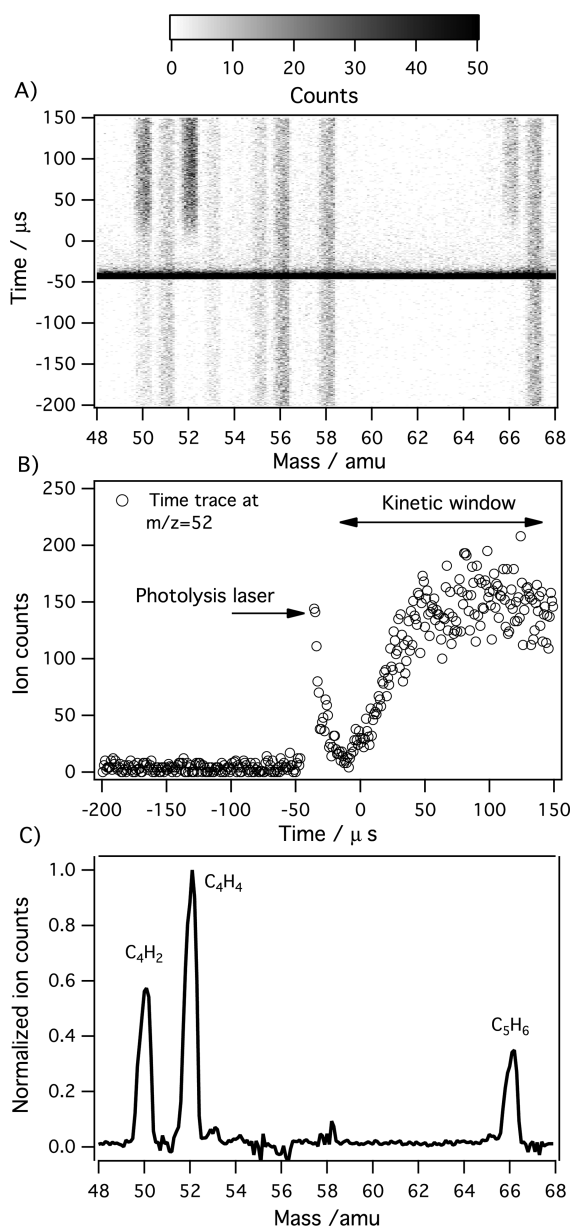


Figure 2. Formation of products as a function of time and mass for the reaction between propene and C_2H . (A) The number of ion counts (grayscale) as a function of time (in μs on the vertical axis) and mass (in amu on the horizontal axis) recorded at a synchrotron ionization energy of 11.25 eV. (B) A time trace obtained by slicing the image vertically from $m/z = 51.5$ to 52.5 . (C) A mass spectrum of the time-dependent reaction products.

the product species at $m/z = 52$ as a function of time at a pressure of 145 mTorr and a temperature of 79 K. Figure 2C is

obtained by subtracting the integrated ion counts before the photolysis laser is pulsed from the integrated ion counts in the kinetic window $t = 0$ and $150 \mu\text{s}$. The resulting mass spectrum reflects time-dependent products that are formed from chemical reactions in the Laval expansion. Ionized reaction products are detected at $m/z = 50, 52$, and 66 .

The product detected at $m/z = 50$ is diacetylene (C_4H_2) formed from the side reaction between C_2H radical and its precursor ($\text{C}_2\text{H} + \text{C}_2\text{H}_2 \rightarrow \text{C}_4\text{H}_2 + \text{H}$) and has been a subject of a previous publication.³⁶ Time dependent products detected at $m/z = 52$ (C_4H_4) and $m/z = 66$ (C_5H_6) are produced by the reaction of C_2H with propene (R2a and R2b, respectively). The time independent signal at $m/z = 58$ is likely caused by acetone from the C_2H_2 cylinder that has not been fully removed by the charcoal filter.

For the reaction between C_2H and ethene, products are detected in mass channel $m/z = 50$ (C_4H_2) and $m/z = 52$ (C_4H_4). Similar to the reaction between C_2H and propene, the mass detected at $m/z = 50$ is attributed to the formation of diacetylene. The product detected at $m/z = 52$ originates from the reaction between C_2H and ethene R1a.

Rate Coefficient Determinations. The bimolecular rate coefficient determinations reported here are made by monitoring the time-dependent formation of the reaction products, rather than the decay of the radical species. The measurements are performed under pseudo-first-order conditions, i.e. the concentration of the radical species is much lower than that of the reactant species ($[\text{C}_2\text{H}] \ll [\text{R}]$). The C_2H radical in the expansion is converted by reactions with the reactant molecule, R, at rate constant k to form reaction products



The reaction between the radical and reactant can lead to the formation of multiple distinct stable products P_m , with accompanying coproducts Y_m such as H-atoms or CH_3 radicals



with:

$$\sum_m k_m = k, \text{ and } m = 1, 2, 3, \dots \quad (4)$$

The formation of product species P_m is now given by

$$\frac{d[\text{P}_m]}{dt} = k_m [\text{C}_2\text{H}]_t [\text{R}] \quad (5)$$

The branching ratio, BR, of product species, P_m , is defined as

$$\text{BR} = \frac{[\text{P}_m]}{\sum_m [\text{P}_m]} = \frac{k_m}{\sum_m k_m} = \frac{k_m}{k} \quad (6)$$

Besides reactions with the reactant species, the radical undergoes side reactions with for example the radical precursor molecule (C_2H_2) or trace amounts of oxygen in the vacuum chamber. In general, one can write that side reactions with molecules M_n excluding the reactant molecule R, at reaction rate k_n form the products X_n and accompanying fragments W_n



with:

$$n = 1, 2, 3, \dots, \text{ and } M_n \neq R \quad (7)$$

The decay of the C_2H radical concentration as a function of time can be expressed by

$$\frac{d[C_2H]}{dt} = -[C_2H](k[R] + \sum_n k_n[M_n]) \quad (8)$$

with the solution to this differential equation

$$[C_2H]_t = [C_2H]_0 \exp[-(k[R] + \sum_n k_n[M_n])t] \quad (9)$$

After substituting eq 9 in eq 5 one can write for the formation of product P_m

$$[P_m]_t = Q_m(1 - \exp[-(k[R] + \sum_n k_n[M_n])t]) \quad (10)$$

with

$$Q_m = \frac{k_m[R][C_2H]_0}{(k[R] + \sum_n k_n[M_n])} \quad (11)$$

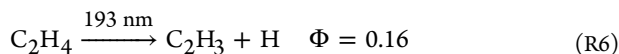
The formation of product species P_m proceeds with the first-order reaction rate coefficient

$$k_{1st} = k[R] + \sum_n k_n[M_n] \quad (12)$$

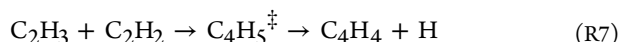
The first-order rate coefficients, k_{1st} , are measured for a set of reactant densities $[R]$. The bimolecular rate coefficient for the reaction between the radical and the reactant, k , is the slope of the values of k_{1st} versus the reactant density, $[R]$. The intercept of the fit on the y axis reflects the sum of all other loss processes that are independent of the reactant concentration.

C_2H + Ethene. Figure 3A depicts the time dependent formation of the product species at $m/z = 52$ for a selected reactant density. The product species are ionized at a synchrotron photon energy of 10.2 eV, prior to being detected in the QMS.

Products formed from side reactions may contribute to the measured time traces of the product species and their contributions to the measured mass channels need to be quantified. Ethene photolysis at 193 nm yields vinyl radicals (C_2H_3) and H atoms with a quantum yield of 0.16⁴⁹



Vinyl radicals produced by C_2H_4 photolysis can subsequently react with C_2H_2 in the expansion to form C_4H_5 which, after losing a hydrogen atom, also yields products in mass channel $m/z = 52$



The absorption cross section of ethene at 193 nm and 140 K is small⁵⁰ ($\sigma_{C_2H_4} = 1 \times 10^{-20} \text{ cm}^2$) compared to the C_2H_2 cross section ($\sigma_{C_2H_2} = 2 \times 10^{-19} \text{ cm}^2$) and the resulting number density of vinyl radicals is low compared to the number density of C_2H radicals in the flow. Furthermore, the reaction of vinyl radicals with C_2H_2 exhibits a barrier to formation of the initial adduct of 4.8 kcal/mol and reaction rates of vinyl radicals are typically very slow, even at high temperatures ($2.6 \times 10^{-14} \text{ cm}^3 \text{ s}^{-1}$ at $T = 630 \text{ K}$).^{8,51} Thus, side reactions of vinyl radicals will

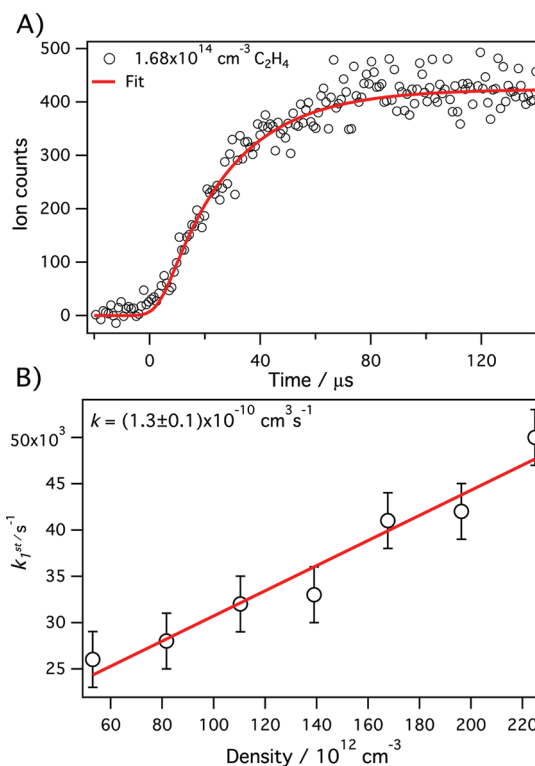


Figure 3. Kinetic measurements for the reaction between C_2H and C_2H_4 . (A) Ion counts in mass channel $m/z = 52$ vs time recorded at a synchrotron photon energy of 10.2 eV. The red line depicts the best fit to the data. (B) Values of k_{1st} as a function of reactant density displayed together with a linear fit to the data.

not interfere with the products formed from the reaction under investigation. Contributions to mass channel $m/z = 52$ of products formed from side reactions of residual acetone from the acetylene cylinder, or acetone photodissociation products, can also be ruled out.

A fit routine is used for obtaining the bimolecular rate coefficient and is described here. First, the routine determines the pre factor Q_m (eq 10) by calculating the average ion counts ranging from 100–125 μs. Subsequently, a fit based on eq 10 is generated with an initial guess for the first-order rate coefficient, k_{1st}^* . Next, the model fit is convoluted with a Gaussian profile with unit area that accounts for the response function of the QMS detector. The sum of the residuals of the convoluted fit and the measured time trace is determined. The routine is repeated for a set of values for k_{1st}^* and the value that results in the lowest sum of residuals is selected as the best fit. In Figure 3A, the best fit is plotted together with the measured time trace at a C_2H_4 density of $1.68 \times 10^{14} \text{ cm}^{-3}$. The fit routine is subsequently repeated for the time traces of the other density settings.

Figure 3B displays the first-order rate coefficients with conservative error bars of $\pm 3000 \text{ s}^{-1}$ as a function of reaction density together with a linear fit to the data. The error in values of k_{1st} originates mainly from the uncertainty in the starting point (t_0) of the reaction, which is obscured by the QMS response. A bimolecular rate coefficient of $(1.3 \pm 0.1) \times 10^{-10} \text{ cm}^3 \text{ s}^{-1}$ for the reaction between C_2H and C_2H_4 is obtained from the weighted linear fit in Figure 3B. The error in the bimolecular rate coefficient depicts the 1σ confidence level. This rate constant is in good agreement with previously measured values. Chastaing et al.³⁰ found that the reaction

between C_2H and C_2H_4 at 112 K using argon as a bath gas proceeds at a rate of $1.59 \pm 0.004 \times 10^{-10} \text{ cm}^3 \text{ s}^{-1}$. Vakhtin et al.³¹ found that the bimolecular rate for C_2H reacting with C_2H_4 is $1.4 \pm 0.4 \times 10^{-10} \text{ cm}^3 \text{ s}^{-1}$ at 103 K and using N_2 as a bath gas.

C_2H + Propene. Products formed from the reaction between propene and C_2H are detected at $m/z = 52$ and 66 (Figure 2). A typical time trace of ion counts detected at $m/z = 52$ for a single reactant density setting is displayed in Figure 4A. Similar

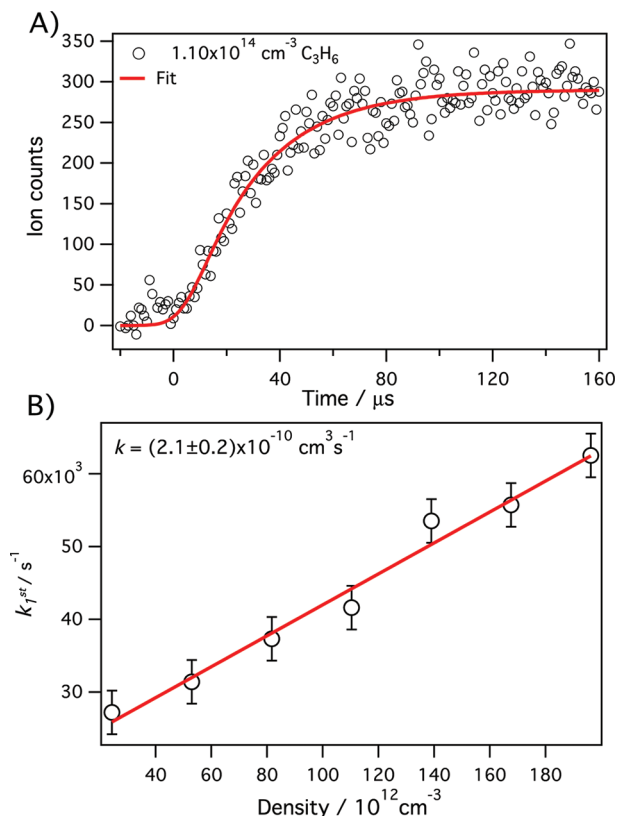
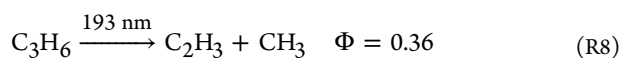


Figure 4. Kinetic measurements for the reaction between C_2H and C_3H_6 . (A) Time-binned reaction product ion counts in mass channel $m/z = 52$ recorded at a synchrotron photon energy of 10.2 eV. The red line depicts the best fit to the data. (B) A plot of the values of k_{1st} as a function of reactant density displayed together with a linear fit to the data.

to the reaction between C_2H and ethene, side reactions may contribute to the observed time traces and need to be quantified.

Propene has an absorption cross section of $7.6 \times 10^{-19} \text{ cm}^2$ at the wavelength of the ArF excimer laser. The quantum yield of C_2H_3 radicals from photolysis of propene is 0.36⁵²



The resulting number density of vinyl radicals in the flow is five times larger than that of the C_2H radicals. Reactions of C_2H_3 with C_2H_2 R7 yields C_4H_4 and can possibly interfere with the reaction under investigation. The bimolecular rate constant of the C_2H_3 radical reacting with C_2H_2 is very slow⁵¹ and a kinetic model shows that the products formed from the side reaction do not contribute significantly to the product observed at $m/z = 52$. Contributions of side reactions involving residual acetone or acetone photoproducts to the either of the expected

mass channels ($m/z = 52$ and 66) can be ruled out. The time traces can thus be used to obtain the rate of the reaction between C_2H and propene.

Figure 4B displays the first-order rate coefficients, k_{1st} , as a function of the reactant density, $[C_3H_6]$. The overall change in reactant density caused by laser photolysis is small (<0.5%) and hence not considered in further analysis. Also indicated in Figure 4B is a weighted linear fit to the data. The bimolecular rate coefficient for the reaction between C_2H and propene is found to be $(2.1 \pm 0.2) \times 10^{-10} \text{ cm}^3 \text{ s}^{-1}$, with the error in the bimolecular rate coefficient displaying the 1σ confidence level. This rate is in good agreement with previously measured rates. Chastaing et al.³⁰ found that, at 112 K using argon as a bath gas, the reaction between C_2H and C_3H_6 proceeds at a rate of $2.35 \pm 0.09 \times 10^{-10} \text{ cm}^3 \text{ s}^{-1}$. Vakhtin et al.³¹ found that the reaction between C_2H and C_3H_6 proceeds at a rate of $2.4 \pm 0.6 \times 10^{-10} \text{ cm}^3 \text{ s}^{-1}$ at 103 K and using N_2 as a bath gas.

Product Branching Ratios. In a separate set of experiments, photoionization spectra were recorded by scanning the photon energy and measuring ion counts at the mass channel under investigation. The resulting photoionization spectra are analyzed to obtain information on the isomers formed from the low temperature chemical reaction.

At a synchrotron photon energy, E , the number of detected ions in a mass channel, I_E , is proportional to the total ionization cross section (σ_E), which is given by

$$I_E \propto \sigma_E = \sum_m \chi_m \sigma_{E,m} \quad (13)$$

where $\sigma_{E,m}$ is the cross section of isomer m at photon energy E and χ_m is the molar fraction of isomer m . The sum over the molar fractions is unity

$$\sum_m \chi_m = 1 \quad (14)$$

Equation 13 allows for branching measurements under the condition that all isomers contributing to a mass channel are ionized.

C_2H + Ethene. The reaction between C_2H and C_2H_4 results in a sole reaction product at $m/z = 52$. A photoionization spectrum of this mass channel, normalized to the number of ion counts at a photon energy of 10.35 eV is shown in Figure 5.

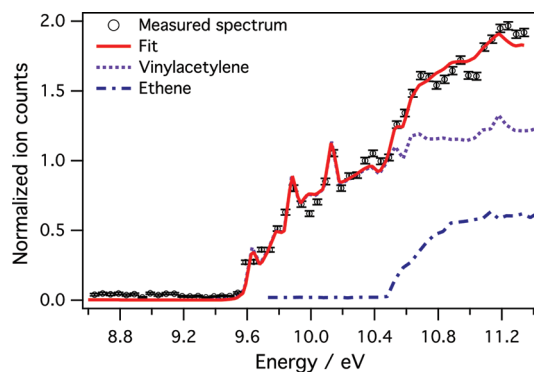
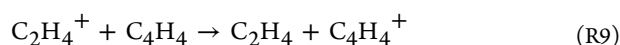


Figure 5. Photoionization spectrum for mass channel $m/z = 52$ plotted together with a model fit and the individual contributions of vinylacetylene and ethene for the C_2H + ethene reaction.

The error bars in Figure 5 comprise the shot noise in the number of detected ion counts (\sqrt{N}).

There are two ionization thresholds visible, located at ~ 9.6 and ~ 10.5 eV. An excellent fit to the measured photoionization spectrum (Figure 5) can be made with contributions of the absolute photoionization spectra of vinylacetylene and ethene taken from measurements by Cool et al.⁵³ The model fit and the individual contributions of ethene and vinylacetylene are also displayed in the Figure 5.

The detection of a large contribution of ethene ($m/z = 28$) at the mass channel of the product species ($m/z = 52$) is surprising and could point to poor mass filtering by the QMS. In this scenario, signals obtained before the photolysis laser is pulsed could be used to subtract the contribution of the reactant molecule, which has a number density much larger than the product species ($[R] > 1000[P_m]$). However, the integrated ethene signal measured before the laser is pulsed accounts for less than 10% of the total ethene contribution to the photoionization spectrum. Thus, the large majority of the ion counts in mass channel $m/z = 52$ that scales with the ethene photoionization spectrum is likely caused by charge-transfer ionization between the neutral reaction product and the ionized reactant molecule, rather than poor mass filtering.



If charge transfer causes the reaction product signal to scale with the reactant ionization cross section, the apparent contribution of the reactant to the photoionization spectrum will depend on the charge transfer cross section of the product species and the reactant. When a kinetic trace is measured above the ionization threshold of the reactant, such as that displayed in Figure 4, there is a contribution of ions formed from charge transfer to the recorded trace. This is not expected to disturb the rate constant determination, since it only adds a contribution to the ion counts with the same time dependence. Modeling efforts are needed to elucidate and possibly reduce the contribution of charge transfer to the observed signal.

Analysis of the photoionization spectrum (Figure 5) points to vinylacetylene as the sole reaction product from C_2H reacting with C_2H_4 . An upper limit of 2% is derived for contributions of the two other C_4H_4 isomers—butatriene and methylenecyclopropene—that are thermodynamically accessible R1a. This is in agreement with earlier findings by Zhang et al.³⁵, who detected vinylacetylene as the sole product from high energy collisions between C_2H and ethene. Furthermore, Kovács et al. found a hydrogen atom yield of 0.94 ± 0.06 ,⁸ which implies that C_4H_4 is the only reaction product.

Our findings are also in agreement with high level quantum mechanical calculations by Woon and Park³⁴ and Krishtal et al.³² Krishtal et al. report that the formation of vinylacetylene is the dominant channel in this reaction. The formation of vinylacetylene, which is exothermic by 26.6 kcal/mol, can most readily occur via direct H-elimination of the initial adduct. Several other two step and three step processes also lead to the formation of vinylacetylene. The thermodynamically accessible formation of $\text{C}_2\text{H}_2 + \text{C}_2\text{H}_3$, which has an exothermicity of 22.2 kcal/mol is only feasible via three or more step processes, which involve 1,3 H-migration or isomerizations with high barriers. The formation of $\text{C}_2\text{H}_2 + \text{C}_2\text{H}_3$ is therefore very unlikely. Woon and Park³⁴ report similar results.

$\text{C}_2\text{H} + \text{Propene}$. Figure 6 shows a photoionization spectrum at $m/z = 52$ normalized to the signal at a photon energy of 10.35 eV and displayed together with error bars that indicate the shot noise in the ion counts. A fit to the photoionization spectrum is made with the absolute photoionization spectrum

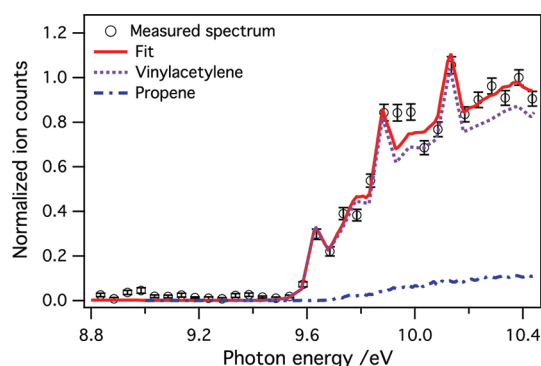


Figure 6. Photoionization spectrum of mass channel $m/z = 52$ formed from the reaction between C_2H and C_3H_6 and normalized at a photon energy of 10.35 eV plotted together with a fit to the data and the individual contributions of propene and vinylacetylene to the fit.

of vinylacetylene and propene. The fit and the individual contributions of vinylacetylene and propene are also displayed in Figure 6. Similar to the reaction between C_2H and ethene, vinylacetylene is the sole C_4H_4 isomer detected at $m/z = 52$ and upper limits of 4% are derived for contributions of other C_4H_4 isomers. The contribution of the ions that scale with the reactant ionization curve is much smaller than for the C_2H reacting with ethene. This could be indicative of a smaller charge transfer cross section for C_3H_6^+ and C_4H_4 .

Figure 7A shows a photoionization spectrum measured for mass channel $m/z = 66$. The spectrum is corrected for

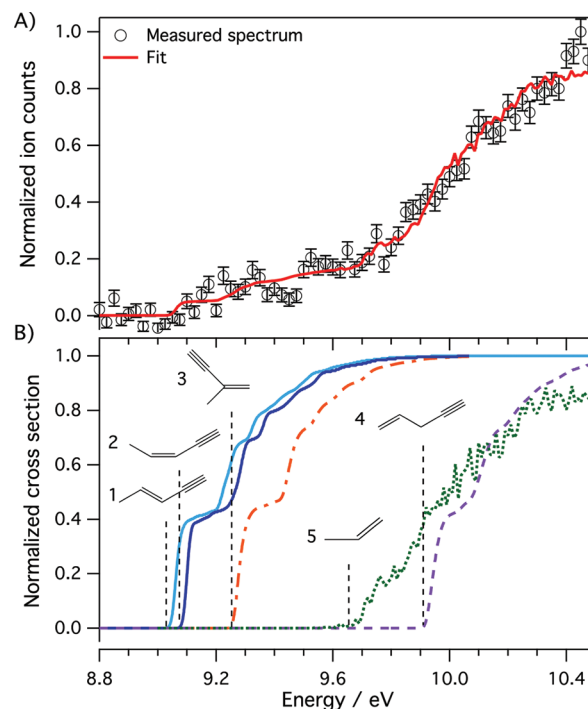


Figure 7. (A) Photoionization spectrum at $m/z = 66$ formed from the reaction between C_2H and C_3H_6 plotted together with a model fit to the data. (B) Simulated photoionization spectra of the C_3H_6 isomers considered in this work plotted together with a measured propene photoionization spectrum. Isomers labels: (1) *trans*-3-penten-1-yne (light blue), (2) *cis*-3-penten-1-yne (dark blue), (3) 2-methyl-1-buten-3-yne (orange dash-dotted), and (4) 4-penten-1-yne (purple dashed). (5) Also displayed in the figure is the photoionization spectrum of the reactant molecule propene (green dotted). Note: All ionization spectra in B are normalized at 11.8 eV.

background counts and plotted together with error bars that display the shot noise in the ion count measurement (\sqrt{N}). An ionization onset is visible at a photon energy of 9.1 eV. The signal at $m/z = 66$ reflects the formation of C_5H_6 isomers from the reaction. Contribution of many C_5H_6 isomers to the photoionization spectrum can be ruled out, since the ionization onset of these species is lower than the onset observed in Figure 7. The remaining C_5H_6 isomers that may possibly contribute to the measured signal are 2-methyl-1-buten-3-yne, *trans*-3-penten-1-yne, *cis*-3-penten-1-yne, and 4-penten-1-yne and are listed in Table 1 together with their ionization energies taken from the literature.⁵⁴

Table 1. Names, Molecular Structures, Literature Values of Ionization Energies (from Bieri et al.⁵⁴), and Calculated Adiabatic Ionization Energies (CBS-QB3 Method, This Work) of the C_5H_6 Isomers Considered Here

Name	Structure	Ionization Energy (eV)	
		Literature	This work
2-methyl-1-buten-3-yne		9.27	9.23
<i>trans</i> -3-penten-1-yne		9.1	9.06
<i>cis</i> -3-penten-1-yne		9.2	9.10
4-penten-1-yne		—	9.93

Photoionization spectra for the isomers listed in Table 1 are not available from the literature, so quantum mechanical calculations are employed to simulate the ionization spectra. The calculated ionization energies are listed in Table 1 and are in very good agreement with literature values, where available. The simulated photoionization spectra normalized at an ionization energy of $E = 11.8$ eV, are plotted in Figure 7B. Also displayed in Figure 7B is the photoionization spectrum of propene measured in the Laval system normalized to the ion yield at 11.8 eV.

In absence of absolute ionization cross sections, and in an attempt to quantify branching ratios from the measured data, a model by Bobeldijk et al.⁴⁸ is employed to estimate the ionization cross sections of the C_5H_6 isomers at a photon energy of 11.8 eV. Within the framework of this model, the cross section of the isomer is computed as the sum of the absorption cross sections of bonds X–Y in the molecule, according to

$$\sigma_{\text{tot}} = \sum \sigma_{X-Y} n_{X-Y} \quad (15)$$


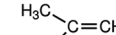
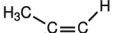
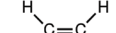
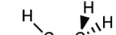
where σ_{tot} is the total cross section of the molecule, σ_{X-Y} is the cross section of bond X–Y, and n_{X-Y} the number of bonds X–Y in the molecule. All four C_5H_6 isomers that possibly contribute to the photoionization spectrum have the same chemical bonds and their ionization cross sections at 11.8 eV are evaluated to be $45 \times 10^{-18} \text{ cm}^2$.

A model fit is made to the measured photoionization spectrum and is displayed in Figure 7A. The onset observed at 9.6 eV is fit by a contribution from the reactant molecule, propene, which accounts for a large fraction ($52\% \pm 10\%$) of the signal observed at $m/z = 66$. The remaining ($48 \pm 10\%$) of the ionization spectrum is fit with C_5H_6 isomers that are

formed from the reaction of C_2H and propene. The geometrical isomers *trans*- and *cis*-3-penten-1-yne fit the ionization onset at 9.1 eV and trace the shape of the photoionization spectrum at energies below 9.3 eV. *Trans*- and *cis*-3-penten-1-yne account for $(27 \pm 8)\%$ of the C_5H_6 product. The spectral resolution of our data is insufficient to discriminate between the two geometrical isomers. A small contribution of 2-methyl-1-buten-3-yne results from the fit, but there is a large error associated with it ($11\% \pm 10\%$). No distinct ionization threshold is observed at 9.9 eV, the onset of 4-penten-1-yne. The quality of the fit, however, improves significantly when this isomer is included and the contribution of 4-penten-1-yne is found to be $(62 \pm 16)\%$. All errors reported here indicate the 1σ confidence level of the fit. Absolute errors in the branching ratios within the C_5H_6 channel may be larger, since these branching ratios are based on simulated ionization spectra and cross sections.

The mass spectrum in the bottom frame of Figure 2 reflects the branching ratio between the two product channels of the reaction between C_2H and propene (eq 6). As pointed out, there is a contribution of propene to each of the mass channels that needs to be subtracted before a branching ratio can be determined. Additionally, the data are corrected for the instrument sensitivity according to eq 3 in order to obtain an accurate branching ratio between the two mass channels. The reaction between C_2H and propene is found to yield $(85 \pm 10)\%$ in the $m/z = 52$ (C_4H_4) channel and $(15 \pm 10)\%$ in the $m/z = 66$ (C_5H_6) channel. The error bar is rather large, since the signal at C_5H_6 is corrected for calculated ionization cross sections, which have large uncertainties. Additionally, the error in the contribution of propene to this channel is large. An overview of the branching ratios of the reaction between propene and C_2H is given in Table 2.

The results presented here can be compared with a recent theoretical study by Woon and Park.³⁴ A detailed C_5H_7 potential energy surface based on data taken from their paper is displayed in Figure 8. The two sites on propene that are available for C_2H addition are the two sp^2 carbon atoms. In their analysis, Woon and Park assume that both addition channels are equally probable; that is, they do not consider steric effects. The lowest pathway to form products from the initial adduct are the direct CH_3 elimination from intermediate 1 in Figure 8, or a 1,2-hydrogen shift in reaction intermediate 2 to form intermediate 3 with subsequent CH_3 elimination. The next lowest pathway they report is the formation of 3-penten-1-yne. This finding is in good agreement with the results presented here, although they do not distinguish between the geometrical isomers of 3-penten-1-yne. Somewhat less favorable is the formation of 4-penten-1-yne, which is observed in the experiments reported here with an abundance larger than the two geometrical isomers of 3-penten-1-yne combined. This could be due to the complication of the analysis caused by the overlapping ionization spectra of 4-penten-1-yne and propene, which is reflected in the large error bars. The formation of C_2H_2 and C_3H_3 is slightly less favorable. This channel has not been observed, because both mass channels are obscured by the strong signals of the radical precursor and reactant molecule, respectively. The formation of cyclopropylacetylene has the largest barrier and is not observed in the experiments reported here. The formation of 2-methyl-1-buten-3-yne from adduct 1 has to compete with the more favorable CH_3 elimination and is found to have a small contribution ($11\% \pm 10\%$) to the measured photoionization spectrum reported here. From their simulations, no stabilization of the adducts or intermediates is

Species	Branching (%)	Isomer	Structure	Branching (%)
C ₄ H ₄	85 ± 10	vinylacetylene		100
C ₅ H ₆	15 ± 10	2-methyl-1-buten-3-yne		62 ± 16
		<i>trans</i> -3-penten-1-yne		27 ± 8 ^a
		<i>cis</i> -3-penten-1-yne		
		4-penten-1-yne		11 ± 10

Reaction coordinate diagram showing the energy profile (kcal/mol) for the addition of propargyl radicals to 2-methyl-1-buten-3-yne. The diagram illustrates the reaction coordinate for three different addition pathways (1, 2, and 3) starting from the reactants (2-methyl-1-buten-3-yne + H·) and ending at the products (1, 2, and 3).

The reactants are 2-methyl-1-buten-3-yne + H·, with an energy level of -28.0 kcal/mol. The products are 1, 2, and 3, with energy levels of -75.7, -59.6, and -71.7 kcal/mol, respectively.

The diagram shows the following energy levels (kcal/mol) for the reactants, transition states, and products:

- Reactants: 2-methyl-1-buten-3-yne + H· (-28.0)
- Transition State 1: -21.3
- Product 1: -75.7
- Transition State 2: -22.3
- Product 2: -59.6
- Transition State 3: -23.3
- Product 3: -71.7
- Intermediate 1: -61.6
- Intermediate 2: -41.7
- Intermediate 3: -42.0
- Intermediate 4: -48.1
- Intermediate 5: -5.1
- Intermediate 6: -14.8
- Intermediate 7: -18.6
- Intermediate 8: -19.9
- Intermediate 9: -24.9
- Intermediate 10: -26.3
- Intermediate 11: -30.2
- Intermediate 12: -35.8
- Intermediate 13: -40.6
- Intermediate 14: -62.5
- Intermediate 15: -71.7

The diagram also shows the chemical structures of the reactants, transition states, and products, including 2-methyl-1-buten-3-yne, 1, 2, and 3, and various intermediates.

expected under the experimental conditions reported here and they predict a yield of $\sim 95\%$ for the formation of vinylacetylene, which is in agreement with this work ($85\% \pm 10\%$).

The reaction between propene and C_2H has been studied at room temperature by measuring the H-atom yield by VUV Ly- α laser induced fluorescence.⁸ Kovács et al. do not detect H-atoms and put an upper limit of 5% for the hydrogen elimination channel. They postulated three reasons for this result: (i) Collisional stabilization of the adduct (ii) 1,2-hydrogen migration forming the more stable $(\text{CH}_3)\text{CH}_2\text{-C}\cdot\text{H-CCH}$ radical is more rapid

dx.doi.org/10.1021/jp301015b | *J. Phys. Chem. A* 2012, 116, 3907–3917

dominant in the C_2H + propene system than in the CN + propene system.

The formation of C_4H_4 is identified as the dominant channel ($85\% \pm 10\%$) for the C_2H + propene reaction. This observation can be explained twofold. First, a steric effect can result in a preferred addition site for the C_2H radical, to form adduct **1**, which preferably loses a methyl group to form C_4H_4 . Second, as postulated by Kovács et al.,⁸ and calculated by Woon and Park³⁴ the 1,2-hydrogen shift to form adduct **3** can be competitive with the accessible H-elimination pathways. Elimination of a methyl group after the 1,2-hydrogen shift results in the formation of vinylacetylene as the main channel. The detection of ($15 \pm 10\%$) in the C_5H_6 product channel reported here versus the upper limit of 5% derived by Kovács et al. can be caused by the pressure difference between the two experiments. The measurements reported by Kovács et al. are performed at a pressure of 50 Torr, which is significantly higher than the pressure in the Laval expansion reported here (145 mTorr). The higher pressure can result in collisional stabilization of the C_5H_7 adduct and can lead to a smaller quantity of detectable H-atoms.

Implications for Titan's Photochemistry. Vinylacetylene is the dominant product of the reactions of ethene and propene with C_2H . The reaction of vinylacetylene with C_2H has recently been studied in a combined experimental theoretical work.⁵⁶ On the basis of their calculations, Zhang et al.⁵⁶ predict that the reaction occurs via barrierless addition of C_2H to vinylacetylene, forming a C_6H_5 adduct. The barrierless addition implies that the reaction will be fast, also at Titan-relevant temperatures. The C_6H_5 adduct subsequently loses a hydrogen atom and the most exothermic product channel of this reaction is the formation of the C_6H_4 isomer *o*-benzyne. Zhang et al.⁵⁶ identified vinylacetylene, hexa-3-ene-1,5-diyne, and *o*-benzyne as reaction products, but could not determine accurate branching ratios. Their calculations predict a branching of $\sim 10\%$ for the formation of *o*-benzyne at low collision energy, when the C_2H radical adds to either the terminal ethylenic or middle ethylenic carbon of vinylacetylene. Accurate branching ratio measurements at low temperatures are needed to confirm the formation of ortho-benzyne under Titan-relevant conditions.

The characteristic yellow haze that shrouds Titan consists of PAHs and large hydrocarbon species that are thought to be formed by photochemical reactions.³ In combustion environments, *o*-benzyne is thought to play a role in the formation of PAHs and soot.^{57,58} Similarly, *o*-benzyne can play a role in the formation of PAHs in low temperature environments. The reactions of C_2H with the alkenes ethene and propene and the subsequent reactions of vinylacetylene with C_2H may thus impact our understanding of the formation of haze in Titan's cold atmosphere.

CONCLUSIONS

Bimolecular rate coefficients have been obtained by measuring the time-resolved formation of product species from the reaction between C_2H and C_2H_4 , and C_3H_6 at 79 K. The measured rate constants ($k_{C_2H_4}(1.3 \pm 0.1) \times 10^{-10} \text{ cm}^3 \text{ s}^{-1}$ and $k_{C_3H_6}(2.3 \pm 0.2) \times 10^{-10} \text{ cm}^3 \text{ s}^{-1}$) are in very good agreement with previously measured values based on the decay rate of the radical species. Furthermore, the product branching ratios for the title reactions have been measured for the first time at low temperature.

The reaction between C_2H and C_2H_4 is found to yield exclusively vinylacetylene via H-atom elimination from the initially formed energetic C_4H_5 adduct. Upper limits of 2% are derived for the energetically accessible isomers butatriene and methylenecyclopropene. This is in agreement with studies performed at room temperature and at high collision energy.^{8,35} Considering these experiments and the work presented here, we conclude that the formed reaction products do not change with temperature.

The products formed from the reaction between C_2H and C_3H_6 are studied for the first time. An initial energetic C_5H_7 adduct forms stable products via two reaction channels; CH_3 loss leading to the formation of vinylacetylene, and H atom elimination leading to the formation of C_5H_6 isomers. The low temperature product branching between these two channels is found to be ($85 \pm 10\%$) for the CH_3 loss channel and ($15 \pm 10\%$) for the H loss channel. The C_4H_4 channel is found to consist of vinylacetylene only, with upper limits of 4% on contributions by other C_4H_4 isomers.

The relative branching for the C_5H_6 isomers is also determined based on photoionization spectrum measurements and simulations. The isomer 4-penten-1-yne is found to be the main contributor and accounts for ($62 \pm 16\%$) of the C_5H_6 channel. A branching ratio of ($27 \pm 8\%$) is derived for the two geometrical isomers *cis*- and *trans*-3-penten-1-yne, while the isomer 2-methyl-1-buten-3-yne is found to have a minor contribution of ($11 \pm 10\%$). No measurements are available from the literature to ascertain the temperature dependence of these branching ratios.

Reactions between the small unsaturated hydrocarbons ethene and propene, and the ethynyl radical are important in the chemical evolution of the cold atmosphere of Saturn's largest moon, Titan. The results presented here unambiguously identify vinylacetylene as the dominant reaction product at low temperatures. The derived branching ratios can be directly used in models that predict the chemical evolution of the Titan's atmosphere.

AUTHOR INFORMATION

Corresponding Author

*E-mail: krwilson@lbl.gov.

Present Address

[§]Department of Chemistry, West Virginia University, Morgantown, West Virginia 26506, United States.

Notes

The authors declare no competing financial interest.

ACKNOWLEDGMENTS

The Advanced Light Source and Chemical Sciences Division (K.R.W. and S.R.L.) are supported by the Director, Office of Science, Office of Basic Energy Sciences of the U.S. Department of Energy under Contract No. DE-AC02-05CH11231 at the Lawrence Berkeley National Laboratory. The support of personnel (J.B. and F.G.) for this research by the National Aeronautics and Space Administration (Grant No. NNX09AB60G) is gratefully acknowledged. Support for J.B. was also obtained from the National Science Foundation Engineering Research Center for Extreme Ultraviolet Science and Technology. The authors would

like to thank Dr. John D. Savee (Sandia National Laboratory) for the many useful discussions.

REFERENCES

- (1) Yung, Y. L.; Allen, M.; Pinto, J. P. *Astrophys. J. Suppl. Ser.* **1984**, *55*, 465–506.
- (2) Wilson, E. H.; Atreya, S. K. *J. Geophys. Res.* **2004**, *109*.
- (3) Lavvas, P.; Coustenis, A.; Vardavas, I. *Planet. Space Sci.* **2008**, *56*, 27–66.
- (4) Krasnopolsky, V. A. *Icarus* **2009**, *201*, 226–256.
- (5) Fulchignoni, M.; et al. *Nature* **2005**, *438*, 785–791.
- (6) Clark, R. N. et al. *J. Geophys. Res.* **2010**, *115*.
- (7) Seki, K.; Okabe, H. *J. Phys. Chem.* **1993**, *97*, 5284–5290.
- (8) Kovács, T.; Blitz, M. A.; Seakins, P. W. *J. Phys. Chem. A* **2010**, *114*, 4735–4741.
- (9) Stahl, F.; v. R. Schleyer, P.; H. F., S. III; Kaiser, R. I. *Planet. Space Sci.* **2002**, *50*, 685–692.
- (10) Goulay, F.; Osborn, D. L.; Taatjes, C. A.; Zou, P.; Meloni, G.; Leone, S. R. *Phys. Chem. Chem. Phys.* **2007**, *9*, 4291–4300.
- (11) Soorkia, S.; Trevitt, A. J.; Selby, T. M.; Osborn, D. L.; Taatjes, C. A.; Wilson, K. R.; Leone, S. R. *J. Phys. Chem. A* **2010**, *114*, 3340–3354 PMID: 20141190.
- (12) Jones, B. M.; Zhang, F.; Kaiser, R. I.; Jamal, A.; Mebel, A. M.; Cordiner, M. A.; Charnley, S. B. *Proc. Natl. Acad. Sci. U.S.A.* **2011**, *108*, 452–457.
- (13) Mebel, A. M.; Kislov, V. V.; Kaiser, R. I. *J. Am. Chem. Soc.* **2008**, *130*, 13618–13629.
- (14) Lavvas, P.; Sander, M.; Kraft, M.; Imanaka, H. *Astrophys. J. Lett.* **2011**, *728*, 80–+.
- (15) Tucker, K. D.; Kutner, M. L.; Thaddeus, P. *Astrophys. J. Lett.* **1974**, *193*, L115–L119.
- (16) Beuther, H.; Semenov, D.; Henning, T.; Linz, H. *Astrophys. J. Lett.* **2008**, *675*, L33–L36.
- (17) Allamandola, L. J.; Tielens, A. G. G. M.; Barker, J. R. *Astrophys. J. Lett.* **1985**, *290*, L25–L28.
- (18) Frenklach, M.; Feigelson, E. D. *Astroph. J.* **1989**, *341*, 372–384.
- (19) Coustenis, A.; Bézard, B. *Icarus* **1995**, *115*, 126–140.
- (20) Coustenis, A.; Salama, A.; Schulz, B.; Ott, S.; Lellouch, E.; h. Encrenaz, T.; Gautier, D.; Feuchtgruber, H. *Icarus* **2003**, *161*, 383–403.
- (21) Waite, J. H.; Young, D. T.; Cravens, T. E.; Coates, A. J.; Crary, F. J.; Magee, B.; Westlake, J. *Science* **2007**, *316*, 870–875.
- (22) Lavvas, P.; Coustenis, A.; Vardavas, I. *Planet. Space Sci.* **2008**, *56*, 67–99.
- (23) Rowe, B. R.; Dupeyrat, G.; Marquette, J. B.; Gaucherel, P. *J. Chem. Phys.* **1984**, *80*, 4915–4921.
- (24) Dupeyrat, G.; Marquette, J. B.; Rowe, B. R. *Phys. Fluids* **1985**, *28*, 1273–1279.
- (25) Atkinson, D. B.; Smith, M. A. *J. Phys. Chem.* **1994**, *98*, 5797–5800.
- (26) Atkinson, D. B.; Jaramillo, V. I.; Smith, M. A. *J. Phys. Chem. A* **1997**, *101*, 3356–3359.
- (27) Lee, S.; Hoobler, R. J.; Leone, S. R. *Rev. Sci. Instrum.* **2000**, *71*, 1816–1823.
- (28) Nizamov, B.; Leone, S. R. *J. Phys. Chem. A* **2004**, *108*, 1746–1752.
- (29) Opansky, B. J.; Leone, S. R. *J. Phys. Chem.* **1996**, *100*, 19904–19910.
- (30) Chastaing, D.; L. James, P.; R. Sims, I.; W. M. Smith, I. *Faraday Discuss.* **1998**, *109*, 165–181.
- (31) Vakhtin, A. B.; Heard, D. E.; Smith, I. W. M.; Leone, S. R. *Chem. Phys. Lett.* **2001**, *348*, 21–26.
- (32) Krishtal, S. P.; Mebel, A. M.; Kaiser, R. I. *J. Phys. Chem. A* **2009**, *113*, 11112–11128.
- (33) Nguyen, H. M. T.; Chandra, A. K.; Carl, S. A.; Nguyen, M. T. *J. Mol. Struct. Theochem* **2005**, *732*, 219–224.
- (34) Woon, D. E.; Park, J.-Y. *Icarus* **2009**, *202*, 642–655.
- (35) Zhang, F.; Kim, Y. S.; Kaiser, R. I.; Krishtal, S. P.; Mebel, A. M. *J. Phys. Chem. A* **2009**, *113*, 11167–11173 PMID: 19522519.
- (36) Soorkia, S.; Liu, C.-L.; Savee, J. D.; Ferrell, S. J.; Leone, S. R.; Wilson, K. R. *Rev. Sci. Instrum.* **2011**, *82*, 124102.
- (37) Sims, I. R.; Queffelec, J.-L.; Defrance, A.; Rebrion-Rowe, C.; Travers, D.; Bocherel, P.; Rowe, B. R.; Smith, I. W. M. *J. Chem. Phys.* **1994**, *100*, 4229–4241.
- (38) Sander, R. K.; Tiee, J. J.; Quick, C. R.; Romero, R. J. *J. Chem. Phys.* **1988**, *89*, 3495–3501.
- (39) Benilan, Y.; Smith, N.; Jolly, A.; Raulin, F. *Planet. Space Sci.* **2000**, *48*, 463–471.
- (40) Samson, J. A. R.; Haddad, G. N.; Masuoka, T.; Pareek, P. N.; Kilcoyne, D. A. L. *J. Chem. Phys.* **1989**, *90*, 6925–6932.
- (41) Samson, J. A. R.; Stolte, W. C. *J. Electron Spectrosc. Relat. Phenom.* **2002**, *123*, 265–276.
- (42) Wood, K. V.; Grange, A. H.; Taylor, J. W. *Anal. Chem.* **1978**, *50*, 1652–1654.
- (43) Frisch, M. J. et al. *Gaussian 03*, revision C.02; Gaussian, Inc.: Wallingford, CT, 2004.
- (44) Montgomery, J. A.; Frisch, M. J.; Ochterski, J. W.; Petersson, G. A. *J. Chem. Phys.* **1999**, *110*, 2822–2827.
- (45) Montgomery, J. A.; Frisch, M. J.; Ochterski, J. W.; Petersson, G. A. *J. Chem. Phys.* **2000**, *112*, 6532–6542.
- (46) Ervin, K. M. *PESCAL, Fortran program*, 2010.
- (47) Ervin, K. M.; Ramond, T. M.; Davico, G. E.; Schwartz, R. L.; Casey, S. M.; Lineberger, W. C. *J. Phys. Chem. A* **2001**, *105*, 10822–10831.
- (48) Bobeldijk, M.; van der Zande, W. J.; Kistemaker, P. G. *Chem. Phys.* **1994**, *179*, 125–130.
- (49) Borrell, P.; Cervenka, A.; Turner, J. W. *J. Chem. Soc. B* **1971**, 2293–2298.
- (50) Wu, C. Y. R.; Chen, F. Z.; Judge, D. L. *J. Geophys. Res.* **2004**, *109*.
- (51) Knyazev, V. D.; Stoliarov, S. I.; Slagle, I. R. *Symp. (Int.) Combust.* **1996**, *26*, 513–519.
- (52) Orkin, V. L.; Huie, R. E.; Kurylo, M. J. *J. Phys. Chem. A* **1997**, *101*, 9118–9124.
- (53) Cool, T. A.; Wang, J.; Nakajima, K.; Taatjes, C. A.; McIlroy, A. *Int. J. Mass Spectrom.* **2005**, *247*, 18–27.
- (54) Bieri, G.; Burger, F.; Heilbronner, E.; Maier, J. P. *Helv. Chim. Acta* **1977**, *60*, 2213–2233.
- (55) Trevitt, A. J.; Soorkia, S.; Savee, J. D.; Selby, T. S.; Osborn, D. L.; Taatjes, C. A.; Leone, S. R. *J. Phys. Chem. A* **2011**, *115*, 13467–13473.
- (56) Zhang, F.; Parker, D.; Kim, Y. S.; Kaiser, R. I.; Mebel, A. M. *Astrophys. J.* **2011**, *728*, 141.
- (57) Friedrichs, G.; Goos, E.; Gripp, J.; Nicken, H.; Schoenborn, J.-B.; Vogel, H.; Temps, F. *Z. Phys. Chem.* **2009**, *223*, 387–407.
- (58) Comandini, A.; Brezinsky, K. *J. Phys. Chem. A* **2012**, in press.